

Advanced Ultrasonic Technology for Freezing Damage Prevention of Concrete Pavement

Ye Sun¹, Xiong (Bill) Yu²⁺, Zhen Liu², Yan Liu², and Junliang Tao²

Abstract: Freezing of concrete can lead to the development of internal crystalline pressure due to the volume expansion of pore liquid. Crack will initialize when such internal pressure exceeds the fracture strength of concrete. Therefore, ensuring the existence of sufficient pore volume to accommodate the volume expansion due to the icing process is important for the prevention of freezing damages to concrete. The volume of air voids of fresh concrete can be measured with standard methods such as ASTM C231. The results, however, do not necessarily indicate the actual pore volume in the hardened concrete, as the pore space continue to evolve as the results of cement hydration. Therefore, determination of the air voids in hardened concrete pavement typically has to involve destructive coring and sophisticated laboratory procedures, i.e., petrological analyses. This paper describes the development of an ultrasonic method for measuring the pore size distribution in hardened concrete specimens. The theoretical basis of the method is developed based on advanced ultrasonic wave scattering model. The model accounts for the attenuation effects of multiple sized air voids. The air voids are treated as either elastic scatterers or cavities, two extreme conditions for their actual physical behaviors. The total attenuations are derived by superimposing the wave attenuation by air void scatterers, coarse aggregates and viscoelastic matrix. The pore size distribution is estimated by a model based inversion analyses procedure. The assumptions of elastic wave scatter and cavity provide the upper and lower bound of the actual air void distribution. The results are encouraging. Factors causing the differences between experimental and theoretical attenuation curves are discussed, which will serve as the thrusts to further develop this technology.

DOI: 10.6135/ijprt.org.tw/2013.6(2).86

Key words: Concrete; Freezing damage; Ultrasonics; Wave scattering.

Introduction

Concrete is widely used for pavement and other infrastructures. As an essential component of infrastructures, the performance and durability of concrete have a profound social economic impact. The multi-scale pore structure in concrete is a key element that determines the performance of concrete such as freezing-thaw durability in cold regions. The liquid water inside the pore space expands about 10% during the icing process. This can produce significant amount of internal pressure on the solid concrete skeleton which can lead to the fracture of concrete. From experience of engineering practice, introduction of well-dispersed air voids helps to prevent concrete from freezing damages; however, high void content (i.e., over 15% in the volume fraction) of air voids can cause significant reduction in the strength of concrete. Therefore, quick identification of air void content and its size distribution is important to ensure its durability in cold regions.

Considerable amount of work has been conducted on the measurement of air voids in concrete. Traditionally, the specific air content in fresh concrete mixture is measured by ASTM standard

methods, including pressure based [1], gravimetric based [2] and volumetric based [3], or petrographic [4] methods. However, these standard methods either are destructive, or cannot be applied to hardened concrete or cannot reach adequate accuracy especially under field conditions.

This paper describes a new method for rapid measurement of pore size distribution and volume fraction based on ultrasonic wave scattering in concrete. The method is an extension of that by Punurai *et al.* [5]. The technical basis is extended from cement to concrete which has a more complex internal structure including viscous matrix, aggregates and air voids. It also gives the idea that could be applied to study the internal structure of other composites.

Background

It has been found that the heterogeneous scatterers including grain and porosity embedded in materials cause energy loss during wave propagation. Various wave scattering models have been developed to describe the ultrasonic attenuation mechanism. The wave attenuation has been proved to be sensitive to the embedded inclusion. Roney [6] modeled the ultrasonic wave propagating through single metal scatterer, and related the attenuation with scatterer size. Ying and Truell [7] studied the scattering by a spherical obstacle of a plane longitudinal wave, and calculated the scattering cross section expressions under different boundary conditions, which shows the total scattered energy caused by different scatterers. Since then, a number of researchers have studied the models of scattering by various scatterers including solid [8-10], fluid [11, 12] and cavity [13-15] with either longitudinal incident wave or transverse wave in elastic medium. Among them,

¹ Department of Electrical Engineering and Computer Science, Case Western Reserve University, Cleveland, OH 44106, USA.

² Department of Civil Engineering, Case Western Reserve University, 2104 Adelbert Road, Bingham 206, Cleveland, OH 44106, USA.

⁺ Corresponding Author: E-mail xxy21@case.edu

Note: Paper presented at the 17th Great Lakes Geotechnical and Geoenvironmental Conference held on May 24th, 2012 at Case Western Reserve University, Cleveland, Ohio, USA. Revised February 5, 2013; Accepted February 6, 2013.

Smith [10] derived an expression for the effect of the grain size distribution in polycrystalline materials on the frequency dependence of the ultrasonic attenuation. For the viscoelastic matrix, the attenuation coefficients are also successfully computed, and the models are applied to characterize matrix composites [16, 17]. Biwa [18] pointed out that the energy loss of wave propagating in viscoelastic composites is caused by scattering by the internal microstructure and absorption of wave energy due to viscoelastic properties. The paper considered both factors and proposed the total wave energy attenuation in inclusion-embedded viscoelastic materials.

The propagation and attenuation of ultrasonic wave in cement-based materials can be modeled based on the theory of wave propagating in viscoelastic composites. The ultrasonic wave attenuation in cement-based materials has already been proposed using theoretical analysis or experimental testing [19-21]. Treiber et al. [22] investigated the influence of sand aggregate on the ultrasonic attenuation in cement-based material. Punurai et al. [5] employed Biwa's model to estimate the average size and the volume fraction of entrained air voids in hardened cement paste. Their research is for air voids of identical size, which does not describe the actual air voids distribution in cementitious materials.

Theoretical Basis of Ultrasonic Wave Scattering in Complex Materials

Ultrasonic Wave Scattered by a Heterogeneous Obstacle.

The theoretical analysis is based on the extension of the elastic wave scattering model proposed by Ying and Truell [7], Johnson and Truell [9]. When an ultrasonic wave which is a plane harmonically periodic longitudinal wave propagates through a heterogeneous spherical inclusion in homogeneous materials, the spatial wave equation can be expressed as Eq. (1),

$$(\lambda + \mu) \nabla \nabla \cdot U + \mu \nabla^2 U = -\omega^2 \rho U \tag{1}$$

where U is the displacement, ω is the angle frequency of the incident wave, λ , μ are Lamé coefficients of the materials, and ρ is the density. In spherical coordinates, the displacement U can be decomposed as two potential functions as Eq. (2),

$$U = -\nabla \phi + \nabla \times \left[\nabla \times \left(\hat{r} r \Pi \right) \right] \tag{2}$$

where ϕ and Π stand for longitudinal and transverse wave. Fig. 1 shows the model. The center of the scatterer is the origin of spherical coordinates. The incident wave is assumed to propagate along the positive z-axis. Then the scattering wave in the matrix and the excitation wave in the scatterer are axially symmetric. Therefore, ϕ and Π satisfy the Helmholtz equations, $(\nabla^2 + k^2)\phi = 0$, $(\nabla^2 + K^2)\Pi = 0$, where k and K are the wave number of longitudinal and transverse wave, $k = [\rho/(\lambda + 2\mu)]^{1/2} = \omega/v_L$, $K = \omega(\rho/\mu)^{1/2} = \omega/v_S$, here v_L and v_S are the wave speed for either kind of wave. Using wave function expansion, the solution of

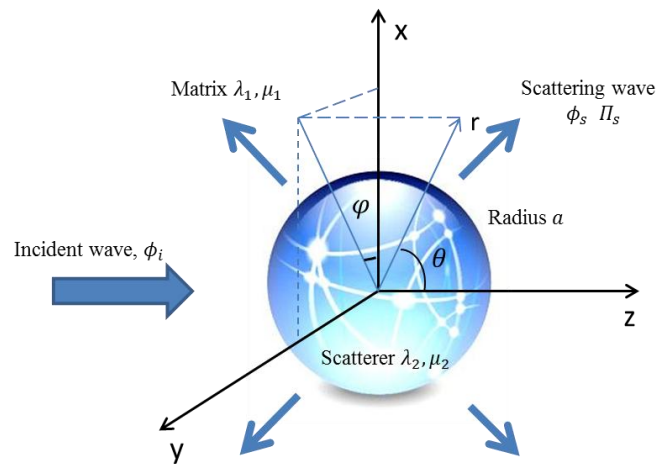


Fig. 1. Model of Ultrasonic Wave Scattered by a Spherical Scatterer.

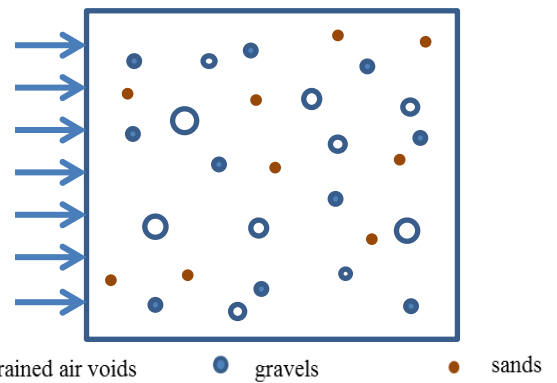


Fig. 2. Model of Wave Propagating Through Concrete Matrix with Multi-scale Air Voids and Identical Gravels and Sands.

scattering wave are $\phi_s = \sum_{m=0}^{\infty} A_m h_m(k_1 r) P_m(\cos \theta)$ for longitudinal

wave and $\Pi_s = \sum_{m=0}^{\infty} B_m h_m(k_1 r) P_m(\cos \theta)$ for transverse wave,

where A_m, B_m are the scattering coefficients which depend on the boundary conditions based on the types and properties of the scatterer.

Ying and Truell [7] introduced the concept of scattering cross section to describe the effects of inclusion (i.e., non-homogenous crystalline particles or air voids) on the wave scattering pattern from the viewpoint of energy. It is defined as the ratio of the total energy scattered per unit time to the energy per unit area carried per unit time by the incident wave [7]. The energy scattered by the scatterer equals to the energy carried away by the scattering wave across the spherical surface. Using the scattering cross section, the effects of inclusions including sands, gravels and air voids on the wave field can be separately represented as a wave attenuation term.

Wave Scattering Through Multiple Entrained Air Voids and Aggregates

With the theory of wave scattering by a single spherical scatterer, a model for ultrasonic wave propagation through concrete specimen

with non-uniform distributed air voids and fine and coarse aggregates, i.e. sands and gravels (Fig. 2), can be developed.

Assuming n_{st} is the number of the inclusions with the radius value a_i distributed per unit volume, i.e., $n_{st} = 3\phi_i / 4\pi a_i^3$, where ϕ_i is the volume fraction corresponding to a specific a_i , then the total wave attenuation caused by scattering can be computed as the superposition of the effects of the scattering by inclusions of each size. Assuming the scatterers do not interfere with each other, which applies when the scatterers are dilute in the matrix. The total attenuation can be expressed as the linear superimposition of attenuation by different sized scatters, Eq. (3),

$$\alpha = (1 - \phi)\alpha_a + \frac{1}{2} \sum_{i=1}^N n_{si} \gamma^{sca}_i \quad (3)$$

where the index i counts as 1, 2, 3, ..., N, referring to the inclusions of each size. where ϕ is the volume fraction of inclusions; α_a is the absorption attenuation of viscoelastic matrix; γ^{sca} is the scattering cross section of a single spherical scatterer; n_s is the number of inclusions distributed per unit volume, $n_s = 3\phi / 4\pi a^3$, and a is the average radius. The unit of attenuation is Neper/m, short as Np/m.

Similarly, when the composites contain more than one type of inclusions, the total attenuation can be computed as Eq. (4).

$$\alpha = (1 - \phi)\alpha_a + \frac{1}{2} \sum_{j=1}^M \sum_{i=1}^N n_{sij} \gamma^{sca}_{ij} \quad (4)$$

where ϕ is extended to the total volume fraction of inclusions; the index j refers to the inclusions of different kinds of materials, M is the total number of material types. For the concrete, j refers to air voids, sands or gravels, and M equals three.

For the entrained air voids in concrete, we believe that there is a distribution $f(r)$ of air void size, where $f(r)$ is the probability density function (PDF). Assuming the air voids in concrete obeys lognormal distribution, and the probability density function is described as Eq. (5):

$$f(r; \mu, \sigma) = \left(1 / r \sqrt{2\pi\sigma^2} \right) \exp \left[-(\ln r - \mu)^2 / 2\sigma^2 \right] \quad (5)$$

where μ and σ are the average and the standard deviation of the radius of air voids. The volume fractions of multiple a_i add up to

the total volume fraction of the air voids, i.e. $\sum_{i=1}^N \phi_{ia} = \phi_a$ or

$\sum_{i=1}^N \phi_{ia} / \phi_a = 1$, where the subscribe a stands for air voids.

Therefore, the value ϕ_{ia} / ϕ_a also obeys a distribution corresponding to that of air void sizes. The possibility of the presence of the air voids with the radius a_i of all the air voids considering the volume.

This relationship is shown as Eq. (6),

$$\phi_{ia} / \phi_a = P_i \frac{4}{3} \pi a_i^3 / \sum_{i=1}^N P_i \frac{4}{3} \pi a_i^3 \quad (6)$$

where P_i is the possibility of appearance of a_i which is assumed to obey lognormal distribution. If the cumulative distribution function is $F(r)$ corresponding to $f(r)$, then we have $P_i = F(a_{i-1}) - F(a_i)$ for numerical computation. It is also applicable for other inclusions. When the method is extended to multiple inclusions, n_{sij} is computed as Eq. (7),

$$n_{sij} = [F(a_{ij}) - F(a_{ij-1})] \phi_j / \sum_{i=1}^N [F(a_{ij}) - F(a_{ij-1})] \frac{4}{3} \pi a_{ij}^3 \quad (7)$$

Substituting Eq. (8) into Eq. (5), the final expression of total wave attenuation in matrix with non-uniform inclusions is Eq. (8).

$$\alpha = (1 - \phi)\alpha_a + \frac{1}{2} \sum_{j=1}^M \sum_{i=1}^N [F(a_{ij}) - F(a_{ij-1})] \phi_j \gamma^{sca}_{ij} / \sum_{i=1}^N [F(a_{ij}) - F(a_{ij-1})] \frac{4}{3} \pi a_{ij}^3 \quad (8)$$

where γ^{sca}_{ij} is the scattering cross section of the inclusions with the material j and the radius a_{ij} . The solution for the scattering cross section varies with different boundary conditions.

Experimental Materials and Procedures

Materials

For concrete specimen, the absorption attenuation α_a caused by concrete matrix can be measured by the experiments on cement-based matrix with no entrained air voids. In reality, this can only be approximately satisfied by measurement on specimens with low air void content. Both concrete and cement mortar specimens were prepared. The cement specimen has a very low air volume that is negligible compared with the concrete specimen. The cement specimen was prepared with Class C cement at the water-cement ratio of 0.3. The concrete specimen belongs to Ohio DOT Class C concrete (Ordinary pavement concrete of 4000 psi). The specimens were cut into cylinders and polished. The thickness of concrete specimen is 45.2cm, which is d in Fig. 3. Table 1 presents the properties of each components including cement, sands and gravels. These parameters help to complete the predicted attenuation.

Experiment Procedure

The experimental ultrasonic wave attenuation measurement was conducted by the spectral ratio technique [24], which was similar to the procedure illustrated by Tokosoz *et al.* [25]. This method was also used by Landis *et al* [19], Punurai *et al.* [21].

Schematic of the equipment and experimental set up is shown in Fig. 3. The ultrasonic system used an ultrasonic wave pulse generator with two 0.5 MHz ultrasonic transducers [20]. The ultrasonic transducers were placed in the opposite sides of the testing specimens. Ultrasonic wave was produced by the coupling the transmitting ultrasonic transducer under the excitation voltage. The wave was received by the receiving transducer after propagating through the specimen. The ultrasonic signals were recorded by use of Picoscope 3424 USB-based oscilloscope. The

Table 1. Material Compositions and Properties of Concrete.

	Cement Paste Matrix	Quartz Sand	Gravel	Air
Volume Fraction	-	8% ^a	6.5% ^a	-
Density (kg/m ³)	2015 ^a	2600 ^b	2670 ^c	-
Longitudinal Velocity (m/s)	3710 ^a	5570 ^b	4435 ^c	340 ^a
Transverse Velocity (m/s)	1990 ^b	3540 ^b	2640 ^c	0 ^a
Average Radius of Aggregates (mm)	-	0.4 ^b	2.1 ^d	-

^aValues are measured from experiments; ^bvalues are taken from Treiber et al. [22]; ^cvalues are taken from Schubert et al. [23]; ^dvalues are taken from the property of Ohio DOT Class C concrete.

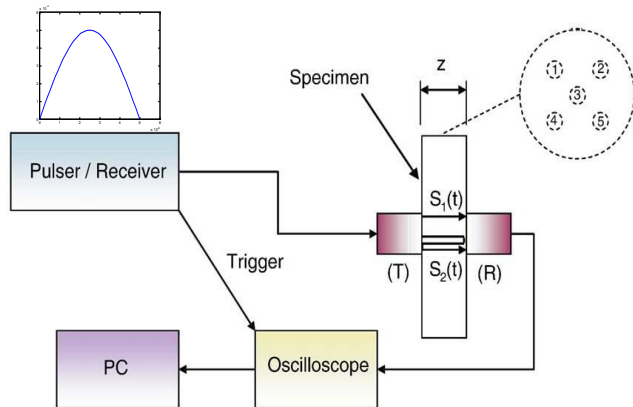


Fig. 3. Equipment and Experiment Procedure.

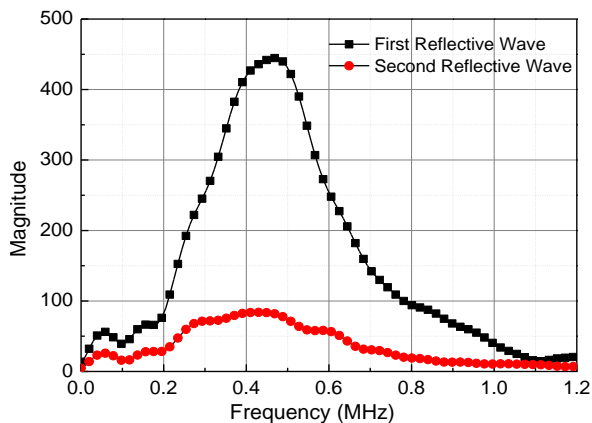


Fig. 4. Spectrum of the First and Second Reflective Wave.

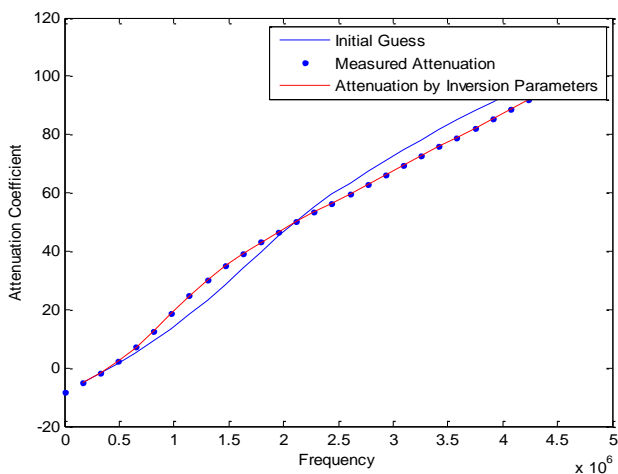


Fig. 5. Curve Fitting of the Cement Paste Attenuation.

signal was acquired with a sampling frequency of 10^7 Hz.

In Fig. 3, $S_1(t)$ is the first transmitted wave measured by the receiving transducer, which means the incident wave travelled across the thickness of the concrete specimen d . $S_2(t)$ is the second round of ultrasonic wave measured by the receiving transducer, which corresponds the incident wave travelled three times distance of d . The frequency spectrum of $S_1(t)$ and $S_2(t)$ can be obtained using the Fast Fourier Transform (FFT) algorithm. Typical spectrums of $S_1(t)$ and $S_2(t)$ are shown in Fig. 4. The signal attenuation caused reduction in the amplitude of wave spectrum. The reduction in the magnitude of $S_2(t)$ compared with $S_1(t)$ is the result of ultrasonic wave attenuation and dispersion.

Use the spectral ratio technique, the total attenuation can be determined by Eq. (9) [5],

$$\alpha(f) = \frac{1}{2d} \left[\ln \left(\frac{S_1(f)}{S_2(f)} \right) - \ln \left(\frac{D(s;d)}{D(s;3d)} \right) \right] \quad (9)$$

where, $\alpha(f)$ is the total attenuation of specimen, d is the thickness of the specimen, S_1 , S_2 are the frequency spectrums of the first and second reflective signals, $D(s;d)$ is the diffraction correction function proposed by Rogers and Van Buren [26].

Results and Analyses

Viscoelastic Attenuation by Cement Matrix

The attenuation by the viscoelastic cement matrix was estimated by analyzing cement paste specimen with low air void content. Results from multiple experiments were averaged and shown in Fig. 5. The trend can be described by curve fitting with higher order terms ignored, i.e.,

$$\alpha_a = 2.4863f + 0.5614 \quad (10)$$

where f is the frequency and the unit is MHz. The expressions were determined in the frequency range of 0.2-0.5 MHz.

Total Attenuation in Concrete Specimen

The total attenuation across the concrete specimen was also measured at multiple locations across the specimen, to reduce the effects by finite size and geometric factors (schematic of locations noted in Fig. 3). Ultrasonic tests were conducted at 15 different points over the concrete specimen. For each test, spectral ratio

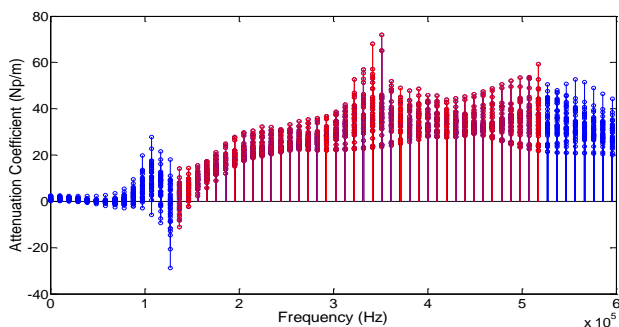


Fig. 6. Attenuation of Experiment Data.

analysis was used to determine the attenuation curve. Fig. 6 shows examples of attenuation curves. The data in 0.15-0.5 MHz range are the frequency range where the matrix attenuation was calibrated. The average measured attenuation coefficient across the concrete specimen was used in the subsequent inversion analysis.

Inverse Analysis

With the measured average total attenuation curve, inversion analysis was conducted to estimate the pore size distribution by comparing the predicted and experimental measured wave attenuation curves (Fig. 7). A forward model was firstly developed to predict the theoretical attenuation based on the ultrasonic wave scattering model describe in the earlier text. An approximation was used in the model, i.e., the sands and the gravels both are assumed to obey the uniform distribution. This means the fine and coarse aggregates are identical respectively. This approximation is also used by Treiber *et al.* [22]. Parameters of the testing specimens in Table 1 were used for the model. The theoretical attenuation model was then compared with the measured attenuation curve. Inversion analysis was conducted using two types of ultrasonic wave propagation models. One treated the entrained air voids as elastic spheres and one treated them as cavities, which represent two extreme physical behaviors. An inversion algorithm was applied to determine the optimal model parameters (the volume fraction of air void ϕ_a and the coefficients of size distribution of air voids, the average μ and standard deviation σ) that result in the minimum error of theoretical prediction and experimental measured attenuation.

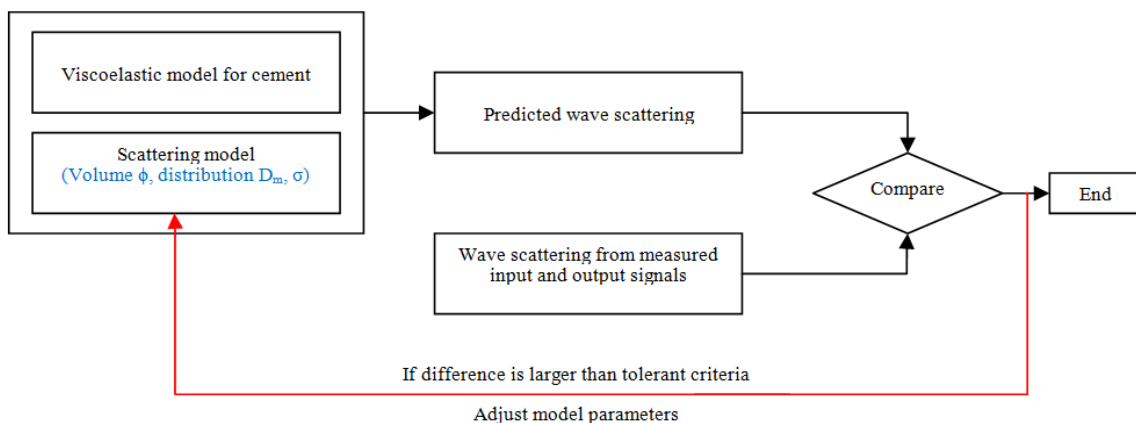


Fig. 7. Schematic of Inversion Analyses Procedure.

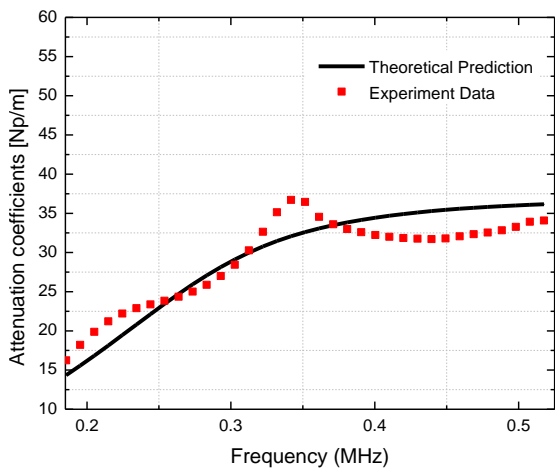
Typical results of inversion analyses using either types of scatters (i.e., elastic-scatterers or cavity scatterers) are shown in Fig. 8. The use of elastic-scatterer model (Fig. 8a) leads to average radius μ of 0.4 mm, the standard derivation of lognormal distribution σ of 1×10^{-6} , and the volume fraction ϕ_a of 6.5%. The use of cavity-scatterer (Fig. 8b) leads to average radius μ of 0.5 mm, standard deviation σ of 0.8×10^{-6} , and the volume fraction ϕ_a of 6.8%.

The distributions of air voids using these two models are shown in Fig. 9. The total volume of air voids fall in the range for this type of concrete (ODOT specification requires the air content of concrete between $6\% \pm 2\%$). The estimated average pore sizes also fall within typical range for concrete.

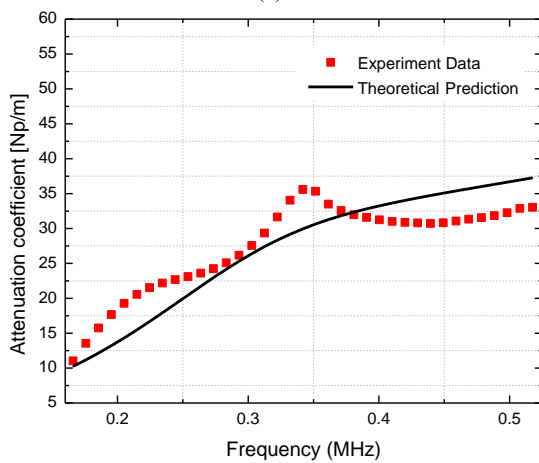
Discussions

There are a few singularity points (peaks) in the experimental measured attenuation curves which lead to large errors between the theoretical predicted and experimental measured values. The phenomenon exists not only in the average attenuation but also in all the other groups of data (shown in Fig. 8). The possible causes of peaks in the experimental attenuation curves include 1) system error, i.e., the characteristics of the ultrasonic transducer, etc.; 2) high concentration of certain sized air voids; 3) multiple wave scattering effects; 4) spherical approximation of embedded inclusions. Experimental and analytical approach was used to identify the most likely causes. The possibilities of these four factors on the observed peaks in the measured attenuation curve are discussed below:

1. The first possible cause of the observation is the system error, i.e., the peaks in the measured attenuation curve might be caused by the characteristics of the ultrasonic system such as the resonant frequency of the ultrasonic transducers. If so, the location of the attenuation peaks should appear at the same frequency, regardless where the transducer is located. In order to inspect this factor, repeated testing was conducted at different locations across the specimens. Three repetitions were conducted at each spot. The measured attenuation curves resemble each other. But the frequencies corresponding to the peaks in the measured attenuation curve changed from one spot to the other spots. Therefore, the peaks are unlikely caused by the experimental error.



(a)



(b)

Fig. 8. Results of Inverse Analysis. (a) Elastic Scatterer Prediction with Experimental Attenuation; (b) Cavity Scatterer Prediction with Experimental Attenuation.

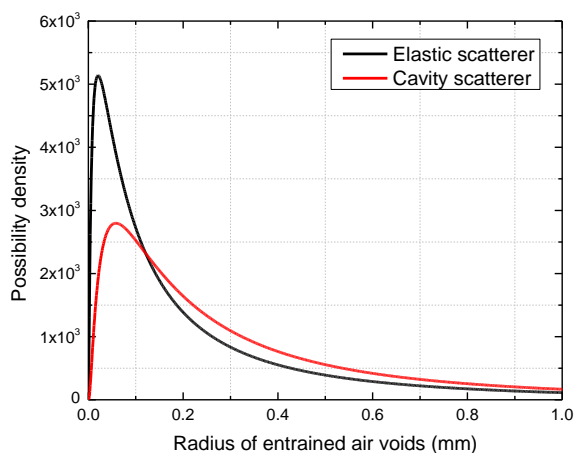


Fig. 9. Size Distribution of Entrained Air Voids Predicted by the Two Models.

2. The second possible cause is the high concentration of specific sized air voids. To inspect the effects of this factor, the wave scattering model simulation was conducted by artificially creating high concentration of narrow ranged air voids. This

however only caused shift of the predicted attenuation curves. No peak was observed. High concentration of specific sized air voids is unlikely to cause the observed peaks in the measured attenuation curves.

3. The third possible cause is the effects of multiple scattering. In the theoretical model only accounts for primary scattering which creates the majority of energy loss. The multiple scattering effects due to a random array of scatterers were neglected for simplicity. Although the multiple scattering effects might have less influence on the total wave attenuation than the primary scattering does, they may determine the details in the attenuation (i.e. peaks). Therefore, the effects of multiple scattering might be a likely cause for the peaks observed in the experimental attenuation curve. Quantitative analysis on the effects of multiple scattering is challenging and requires further investigation.
4. The observation can also be due to the spherical approximation of embedded inclusions. In the theoretical analysis, the inclusions were assumed to be ideal sphere, therefore the derived formulation of scattering cross section is smooth. However, when the scatterers are not spherical (e.g. with edges), the curve might not be smooth, since the surface integration will be applied not on the spherical surface but an arbitrary surface. The shape of the embedded inclusion might a possible cause of the observed peak in the measured attenuation curves.

Conclusion

Ensuring sufficient amount of air voids in concrete is crucial for the durability of concrete in cold regions. There are limitations of conventional ways for air voids assessments of hardened concrete. This paper describes the development of ultrasonic technology for air void measurements. The technical basis is an advanced ultrasonic wave scattering model for the ultrasonic wave attenuation in complex heterogeneous materials. The wave attenuation effects of the air voids are solved by modeling them either as elastic scatterers or cavity scatterers. These represent the extreme wave scattering behaviors for void embedded in homogeneous materials. The wave attenuation of matrix is modeled with viscoelastic model. The total wave attenuation is determined by superimposing the absorption attenuation and inclusion scattering (air voids, sands, and gravels) mechanisms. Experiments were conducted to validate the proposed method. From these the volume of air void and their size distribution is estimated from parameters determined by inversion analyses. Both fall within reasonable range for concrete. Factors causing the peaks in the experimental attenuation curve are discussed.

Acknowledgements

The support from ASNT on this study is highly appreciated.

References

1. ASTM C231 (1991). Standard test method for air content of

- freshly mixed concrete by the pressure method, American Society of Testing and Materials, Philadelphia, PA, USA.
2. ASTM C138 (1992). Standard test method for unit weight, yield, and air content (gravimetric) of concrete, American Society of Testing and Materials, Philadelphia, PA, USA.
 3. ASTM C173 (1994). Air content of freshly mixed concrete by the volumetric method, American Society of Testing and Materials, Philadelphia, PA, USA.
 4. ASTM C457-98 (2000). Standard test method for air content of freshly mixed concrete by the volumetric method, American Society of Testing and Materials, Philadelphia, PA, USA.
 5. Punurai, W., Jarzynski, J., Qu, J., Kurtis, K.E., and Jacobs, L.J. (2006). Characterization of entrained air voids in cement paste with scattered ultrasound, *NDT&E International*, 39, pp. 514-524.
 6. Roney, R. K. (1950). The influence of metal grain structure on the attenuation of an ultrasonic acoustic wave, *PhD Thesis*, California Institute of Technology, Pasadena, CA, USA.
 7. Ying, C. F., and Truell, R. (1956). Scattering of a plane longitudinal wave by a spherical obstacle in an isotropically elastic solid, *Journal of Applied Physics*, 27, pp. 1086-1097.
 8. Waterman, P. C., and Truell, R. (1961). Multiple scattering of waves, *Journal of Mathematical Physics*, 2, pp. 512-537.
 9. Johnson, G., and Truell, R. (1965). Numerical computations of elastic scattering cross sections, *Journal of Applied Physics*, 36, pp. 3466-3475.
 10. Smith, R. L. (1982). The effect of grain size distribution on the frequency dependence of the ultrasonic attenuation in polycrystalline materials, *Ultrasonics*, 20, pp. 211-214.
 11. Einspruch, N. G., and Truell, R. (1960). Scattering of a plane longitudinal wave by a spherical fluid obstacle in an elastic medium, *Journal of Acoustic Society of American*, 32, pp. 214-219.
 12. Einspruch, N. G., Witterholt, E. J., and Truell, R. (1960). Scattering of a plane transverse wave by a spherical obstacle in an elastic medium, *Journal of Acoustic Society of American*, 31, pp. 1806-1818.
 13. Tittmann, B. R., Cohen, E. R., and Richardson, J. M. (1978). Scattering of longitudinal wave incident on a spherical cavity in a solid, *Journal of Acoustic Society of American*, 63, pp. 68-74.
 14. Jain, D. L., and Kanwal, R. P. (1978). Scattering of P and S waves by spherical inclusions and cavities, *Journal of Sound and Vibration*, 57, pp. 171-202.
 15. Nair, S. M., Hsu, D. K., and Rose, J. H. (1989). Porosity estimation using the frequency dependence of the ultrasonic attenuation, *Journal of Nondestructive Evaluation*, 8, pp. 13-26.
 16. Gaunaurd, G. C., and Uberall, H. (1978). Theory of resonant scattering from spherical cavities in elastic and viscoelastic media, *Journal of Acoustic Society of American*, 63, pp. 1699-1712.
 17. Beltzer, A. I., and Brauner, N. (1988). Wave propagation in random particulate composites: A modification of the Foldy-Lax theory, *Acoustica*, 65, pp. 156-162.
 18. Biwa, S. (2001). Independent scattering and wave attenuation in viscoelastic composites, *Mechanical Materials*, 33, pp. 635-647.
 19. Landis, E. N., and Shah, S. P. (1995). Frequency-dependent stress wave attenuation in cement-based materials, *Journal of Engineering Mechanics*, 121, pp. 737-743.
 20. Philippidis, T., and Aggelis, D. (2005). Experimental study of wave dispersion and attenuation in concrete, *Ultrasonics*, 43, pp. 584-595.
 21. Punurai, W., Jarzynski, J., Qu, J., Kim, J.Y., Jacobs, L.J., and Kurtis, K.E. (2007). Characterization of multi-scale porosity in cement paste by advanced ultrasonic techniques, *Cement and Concrete Research*, 37, pp. 38-46.
 22. Treiber, M., Kim, J. Y., Qu, J., and Jacobs, L. J. (2010). Effects of sand aggregate on ultrasonic attenuation in cement-based materials, *Materials and Structure*, 43, pp. 1-11.
 23. Schubert, F., Lausch, R., and Wiggenhauser, H. (2003). Geometrical effects on impact-echo testing of finite concrete specimens, *International Symposium of Non-Destructive Testing in Civil Engineering*, Paper No. 39, Berlin, Germany.
 24. Sears, F. M., and Bonner, B. P. (1981). Ultrasonic attenuation measurement by spectral ratios utilizing signal processing techniques, *IEEE Transactions on Geoscience and Remote Sensing*, GE-19, pp. 95-99.
 25. Toksoz, M. N., Johntson, D. H., and Timur, A. (1979). Attenuation of seismic waves in dry and saturated rocks: I. Laboratory measurements, *Geophysics*, 44, pp. 681-690.
 26. Rogers, P. H., and van Buren, A. L. (1974). An exact expression for the Lommel diffraction correction integral, *Journal of Acoustic Society of American*, 55, pp. 724-728.